RESEARCH PAPER

CrossMark

Influence of welding parameters on pit initiation and pit growth in welded joints of X5CrNi18-10 stainless steel

Bore V. Jegdić [1] · Biljana M. Bobić [1] · Bojana M. Radojković [1] · Behar Alić [2]

Abstract

The influence of welding parameters on the resistance to pitting corrosion in welded joints of X5CrNi18-10 stainless steel was studied. Welding was performed by a TIG procedure in a shielding gas containing different amounts of nitrogen. The welding speed, the deposition rate of the filler wire, and the shielding gas flow rate were constant, which allowed the nitrogen content in the weld metal to be directly dependent on the nitrogen content in the shielding gas. It was shown that welding current and arc energy had a significantly lower influence on the resistance to pit formation and pit growth, than the nitrogen content in the shielding gas. Pitting corrosion testing was conducted using the potentiodynamic polarization method. The resistance to pit formation increases with the increase in nitrogen content in the weld metal, while the resistance to pit growth decreases. The microstructure of the weld metal becomes more homogeneous in the presence of nitrogen and the distribution of chromium more uniform, which leads to the increased resistance to pit formation. Also, due to the formation of ammonia ions, the pH value of the solution within the pit is higher than in the bulk solution, which also increases the resistance to pit formation.

Keywords Pitting corrosion · Austenitic stainless steels · Welded joints · Nitrogen · Electrochemical methods

1 Introduction

Stainless steels are iron-based alloys containing at least 10.5% chromium. They are corrosion resistant because of the formation of surface passive film that separates the metal from the corrosive environment. Chromium is the most important alloying element for passive film formation. The content of chromium in the passive film is much higher than its content in the bulk metal [1].

Pitting corrosion usually occurs in welded joints (weld metal and heat-affected zone, HAZ) of austenitic stainless steels in chloride solutions [2]. Pitting corrosion resistance of the weld metal can be significantly increased using the filler metal with a higher concentration of alloying elements (Cr and Ni) than that in the base metal.

In the case of nonstabilized austenitic stainless steels, the arc energy input during welding leads to the precipitation of chromium carbides on the grain boundaries in the HAZ. The influence of arc energy on the pitting corrosion in welded joints (formed without nitrogen in the shielding gas) of X5CrNi18-10 austenitic stainless steel was examined in detail in our previous paper [3]. During pit formation, an electrochemical corrosion cell is formed between the passive surface of the metal and the active surface at the pit bottom. The pitting corrosion can be explained by a localized acidification model, due to metal ion hydrolysis [4]. For austenitic stainless steels exposed to neutral 0.5 M NaCl, the pH value inside the pit was found to be pH < 1 [5]. The presence of chloride ions prevents the repassivation of the metal surface at the pit bottom [6]. There is a linear dependence between the pitting corrosion resistance of austenitic stainless steels and the chloride ion concentration. As the concentration of chloride ions increases, the value of pitting potential E_{pit} decreases [5]. Pitting corrosion of welded joints of austenitic stainless steels in chloride solutions occurs in three stages: nucleation,

---

✉ Bore V. Jegdić
borejegdic@yahoo.com

1   Institute of Chemistry, Technology and Metallurgy, University of Belgrade, Njegoseva 12, Belgrade, Serbia

2   Metallurgical Institute "Kemal Kapetanovic", Travnicka cesta 7, Zenica, Bosnia and Herzegovina

metastable pit growth, and stable pit growth [7]. Metastable pits are repassivated after a relatively short time. The repassivation of metastable pits is related to the rupture of passive film covers and to the dilution of the local pit environment [6].

The methods for testing pitting corrosion and other corrosion forms in welded joints of stainless steels are described in [8, 9]. The pitting corrosion resistance in welded joints of austenitic stainless steels can be determined by an electrochemical potentiodynamic method, in accordance with ASTM G61 standard [10]. In addition to the pitting potential E_{pit}, it is possible to determine the value of the protection potential E_{prot}, i.e., the value of the potential when the formed pits stop to grow. At potentials more positive than E_{pit}, pits are formed and grow continuously. In the potential region between E_{pit} and E_{prot}, previously formed pits grow. At potentials more negative than E_{prot}, pits are repassivated and stop to grow. The potential of the metastable pit formation E_{mpit} can be also determined using the potentiodynamic method [11]. The value of the $E_{pit} - E_{corr}$ difference and the value of $E_{pit} - E_{prot}$ difference can be taken as indicators of the resistance to pit formation and to pit growth, respectively [12–16]. Corrosion potential E_{corr} is the open-circuit potential, which is spontaneously established on the surface of stainless steels in a test solution. The resistance to pit formation increases if the difference $E_{pit} - E_{corr}$ is increased. However, the resistance to pit growth decreases if the difference $E_{pit} - E_{prot}$ is increased.

Frankel, Li, and Scully proposed the new theory of pitting corrosion in 2017 [17]. In accordance with the theory proposed, pit formation in a stainless steel is more difficult when the welded joint microstructure is resistant to pitting corrosion or when pitting corrosion occurs in a less aggressive corrosive environment, and vice versa. In that case, the resistance of the welded joint to pit growth is higher, i.e., pits are easily repassivated. For example, in the chemical processing industry, welded joints of austenitic stainless steels are often exposed to the influence of an aggressive corrosive environment (the presence of chlorides, elevated temperatures, etc.). The increase in the resistance of the weld metal (of X5CrNi18-10 stainless steel) to pit formation which leads to a decrease in its resistance to pit growth is considered in this paper.

It is known that nitrogen in austenitic and duplex stainless steels, especially in the presence of molybdenum, favorably influences the resistance to pitting corrosion [18]. According to [19, 20], nitrogen in a pit is transformed into ammonia ions during the pitting corrosion of stainless steels. In line with the proposed assumption, the ammonia ions prevent the decrease of the pH value in the pit [19, 20].

A solution with a pH value higher than the critical is formed in the pit in the presence of ammonia ions. Consequently, the repassivation of the formed pit is easier in the early stage. The formation of stable pits occurs at pH values lower than the critical pH value.

The nitrogen effect on pitting corrosion resistance can be attributed to the accumulation of nitrogen beneath the passive film, according to [21]. This nitrogen can be transformed directly into ammonia ions. In the presence of nitrogen in austenitic stainless steels, the formed nitrates inside the pit can also inhibit pitting corrosion [21]. The inhibiting role of nitrates is based on the acid consumption and formation of ammonia ions.

The favorable influence of nitrogen on the pitting corrosion resistance has been observed in austenitic and duplex stainless steels containing nitrogen as an alloying element. Welding of austenitic stainless steels in a shielding gas with nitrogen was considered in [22], while welding of duplex stainless steels was studied in [23, 24].

The aim of this paper was to examine the influence of shielding gas composition and the influence of other welding parameters on the pit initiation and pit growth in the welded joints of X5CrNi18-10 austenitic stainless steel. Welding was carried out at a constant value of the welding speed, the deposition rate of the filler wire, and the shielding gas flow rate, which allowed the nitrogen content in the weld metal to be directly dependent on the nitrogen content in the shielding gas. All this resulted in microstructural transformations in the welded joint and in changes in the pitting corrosion resistance. The aim of this work was also to confirm the proposed new theory of pitting corrosion [17] on the basis of the obtained results.

2 Experimental

2.1 Materials and welding parameters

The welding of X5CrNi18-10 stainless steel was performed by tungsten inert gas (TIG) welding using the welding equipment with an automatic wire feeder.

The welding samples were in the form of a plate (237 × 150 × 6 mm). Tungsten electrodes WT 20, alloyed with 2.0% thorium (2.4 mm in diameter), were used for welding.

The values of the welding parameters are given in Table 1. The values of the deposition rate of the filler wire, the welding speed, and the gas flow rate are maintained constant. In this way, the amount of nitrogen in the weld metal depends solely on the nitrogen amount in the shielding gas. In addition, the results shown in Table 1 indicate a good correlation between the welding current and the arc energy.

After welding, the welded joints were examined using nondestructive test methods (visual inspection, penetrants, and radiography). For further testing, welded joints of high quality were selected in accordance with ISO 5817 [25]. The dimensions of the seam groove are shown in Fig. 1a, and the welding layer sequence is shown in Fig. 1b.

Table 1 Welding parameters

Shielding gas	I (A)	Layer	U (V)	v_{wire} (m/min)	$v_{welding}$ (cm/min)	v_{gas} (l/min)	E (kJ/mm)	
							E_{single}	$E_{average}$
Ar	130	1	9.8	0.30	5	15	1.53	1.79
		2	12.4	0.26			1.93	
		3	12.3	0.18			1.92	
Ar + 1.25 vol% N_2		1	9.8	0.30	5	15	1.53	1.93
		2	12.4	0.26			1.93	
		3	15.0	0.18			2.33	
Ar + 2.50 vol% N_2		1	10.8	0.30	5	15	1.68	1.97
		2	12.9	0.26			2.02	
		3	14.2	0.18			2.22	
Ar	150	1	11.5	0.30	5	15	2.07	2.42
		2	13.9	0.26			2.50	
		3	15.0	0.18			2.70	
Ar + 1.25 vol% N_2		1	10.7	0.30	5	15	1.93	2.31
		2	13.1	0.26			2.37	
		3	14.6	0.18			2.63	
Ar + 2.50 vol% N_2		1	10.3	0.30	5	15	1.85	2.34
		2	13.3	0.26			2.40	
		3	15.5	0.18			2.78	

I welding current, U arc voltage, v_{wire} deposition rate of the filler wire, v_{gas} gas flow rate, $v_{welding}$ welding speed, E arc energy

The chemical composition of the base metal, welding wire, and weld metal was determined. The content of individual elements was determined in accordance with relevant standards. The content of C and S was determined by the gas-volumetric method; the P content was determined by the photometric method; the Si content was determined by the gravimetric method; and the content of Cr, Ni, Mo, and Mn was determined by the atomic absorption spectrophotometric method. The content of N was determined by the titrimetric method in accordance with ISO 10702 [26]. The chemical composition of the base metal, welding wire, and weld metal tests is given in Tables 2 and 3.

Argon and argon with 1.25 vol% nitrogen and 2.50 vol% nitrogen were used as shielding gas. The welding current was 130 and 150 A. The results in Table 3 show the increased nitrogen content in the weld metal at higher nitrogen content in the shielding gas.

It can be noticed that the concentration of Cr and Ni in the weld metal is lower than the prescribed concentration of these elements in the welding wire (Tables 2 and 3). This is due to burn-off losses during welding [28].

2.2 Ferrite number

The content of δ-ferrite (ferrite number, FN) in the weld metal was determined using Feritscope MP30E. Measurement of the ferrite number was performed at the measuring points distributed in the form of a network (measuring directions and measuring levels). Measuring directions (I to XI in Fig. 2) are arranged along the length of the weld metal at a distance of 20 mm. Measuring levels (− 10 to 10 in Fig. 2) are arranged parallel to the axis of the weld metal, at a distance of 10 mm. The axis representing the zero level is the longitudinal axis of the weld metal, and the numbering is performed symmetrically on both sides of the weld metal in the opposite directions, denoted by "+" and "−" (Fig. 2). The results of ferrite number measurements are given in Tables 4 and 5.

Table 5 shows that increased content of nitrogen in the shielding gas results in a reduction in the ferrite number value, i.e., a decrease in the δ-ferrite content in the weld metal.

Fig. 1 **a** The dimensions of the seam groove before welding (mm). **b** The welding layer sequence
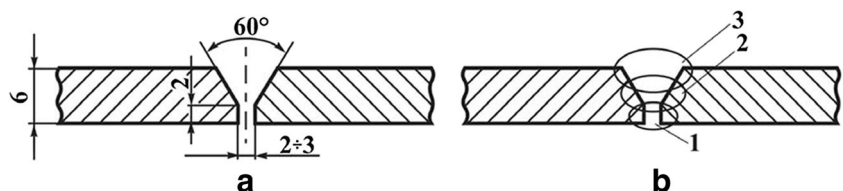
Table 2 Chemical composition of the base metal and the welding wire, mass %

Material	C	Si	Mn	P	S	Cr	Ni	Mo	N
X5CrNi18-10	0.04	0.34	1.20	0.007	0.006	18.8	9.5	0.22	0.05
MW 308 LSi[*]	0.03	0.80	1.90	0.007	0.007	20.1	9.90	0.07	0.06

[*] G 19 9L Si according to EN 12072 [27]

2.3 Hardness

The hardness measurements of the welded joints were carried out using the Zwick device. The measurements were performed in the weld metal, in the HAZ, and in the base metal. The scheme of the measuring points is shown in Fig. 3. The results of hardness measurements are given in Table 6. The signs "− 2*" and "2*" refer to the average values of the results of the hardness measurements close to the fusion line.

Table 6 shows that the hardness of the welded joint is slightly lower than the hardness of the base metal. The lowest hardness values were measured in the HAZ. The dependence of the welded joint hardness on the welding current level, i.e., on the arc energy input, cannot be noticed. Also, the presence of nitrogen in the shielding gas does not significantly affect the hardness of the welded joint.
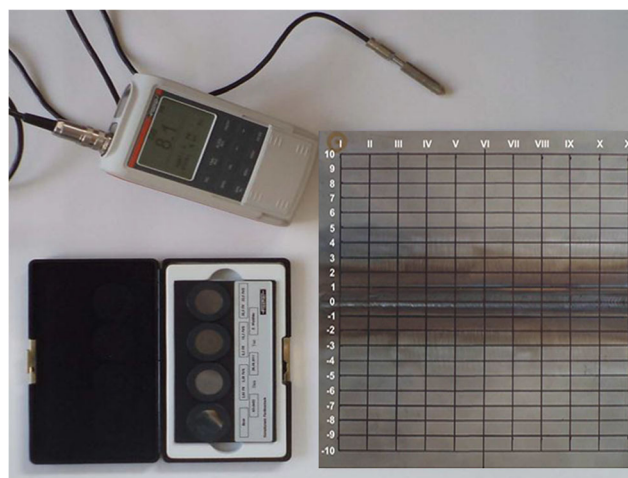
The microstructure of the weld metal was studied using an optical microscope Olympus PMG3. Adler's etching reagent was used to reveal weld metal microstructures.

2.4 Pitting corrosion testing

The potentiodynamic polarization method was used for testing pitting corrosion by a Bio-Logic SP-200 potentiostat/galvanostat. The tests were carried out in the weld metal of the welded joints. The test samples were wet ground with a progressively finer abrasive paper (400 to 1000 grit), and then degreased in ethanol, washed with distilled water, and dried in the air. A three-electrode electrochemical cell with a reference electrode (saturated calomel electrode, SCE) and an auxiliary electrode (Pt mesh) was used for the tests. The sample surface (weld metal) exposed to the test solution was 0.785 cm^2. The tests were carried out at room

Fig. 2 Feritscope, etalons for calibration, and welded joint sample with grid for FN measurements

temperature, in the test solution: 0.3 M NaCl + 0.1 M Na$_2$SO$_4$. Anodic polarization curves were recorded at a sweep rate of 0.5 mV s^{-1}. After reaching the current density of 500 μA cm^{-2}, the polarization direction was reversed. The value of E_{pit} and the value of E_{prot} were determined from the recorded polarization curves. A characteristic polarization curve is shown in Fig. 4. The pitting potential E_{pit} is defined as a potential corresponding to the anodic current density of 10 μA cm^{-2} in the region of stable pit growth, according to ISO 15158 [29]. The protection potential E_{prot} is the potential when the pit growth practically stops. Determination of pit formation indicator ($E_{pit} − E_{corr}$) and pit growth indicator ($E_{pit} − E_{prot}$) is shown in Fig. 4.

2.5 SEM/EDS measurements

The morphology of welded joints on the X5CrNi18-10 austenitic stainless steel surface after pitting corrosion tests was analyzed by a scanning electron microscope (SEM) JEOL JSM-6610LV, equipped for energy-dispersive spectroscopy (EDS) measurements. The microstructural analysis and the determination of the chemical composition of the austenite and ferrite phases in the weld metal were performed using the same SEM device. Several measurements of the chemical composition were performed for the ferrite and austenite phase in the weld metal.

Table 3 Chemical composition of the weld metal, mass % ($I = 130$ A)

	C	Si	Mn	Cr	Ni	Mo	N
Weld metal (Ar)	0.023	0.51	1.50	18.50	8.60	0.16	0.056
Weld metal (Ar + 1.25 vol% N$_2$)	0.042	0.51	1.48	18.40	8.60	0.18	0.130
Weld metal (Ar + 2.50 vol% N$_2$)	0.029	0.51	1.43	19.00	8.40	0.19	0.190

Table 4 Ferrite number, FN ($I = 130$ A, Ar + 1.25 vol% N_2)

Measuring level	Measuring direction											FN_{av}
	I	II	III	IV	V	VI	VII	VIII	IX	X	XI	
3	0.44	0.37	0.35	0.37	0.39	0.42	0.41	0.38	0.36	0.37	0.42	0.39
2	0.40	0.35	0.39	0.44	0.44	0.48	0.45	0.44	0.38	0.36	0.39	0.41
1	0.41	0.41	0.44	0.47	0.46	0.48	0.46	0.50	0.43	0.45	0.42	0.45
0	3.40	2.60	2.80	2.80	2.40	2.50	2.50	2.90	3.30	3.40	4.10	2.97
− 1	0.47	0.46	0.57	0.56	0.56	0.53	0.51	0.53	0.50	0.39	0.46	0.50
− 2	0.54	0.45	0.49	0.57	0.59	0.62	0.58	0.59	0.48	0.46	0.51	0.53
− 3	0.49	0.45	0.43	0.45	0.49	0.48	0.50	0.44	0.41	0.46	0.58	0.47

3 Results and discussion

3.1 Microstructure

Figure 5 shows the microstructure of the weld metal (revealed using Adler's etchant) for the welding current of 130 A, while Fig. 6 shows the microstructure of the weld metal for the welding current of 150 A. The light phase on these figures is the austenite phase, and the dark phase is the δ-ferrite phase. It can be seen that the content of δ-ferrite decreases with increasing nitrogen content in the shielding gas, for both welding currents [18]. This is in accordance with the measured values of ferrite number (Tables 4 and 5).

3.2 Pitting corrosion

The results of pitting corrosion tests are shown in Fig. 7. The values of pitting corrosion parameters (E_{corr}, E_{pit}, and E_{prot}) are also indicated in Fig. 7.

The relatively small current peaks on the polarization curves (Figs. 4 and 7) are caused by the appearance of metastable pits on the stainless steel surface. A gradual current increase to a certain value, followed by a sudden current decrease, indicates the appearance of metastable pits and their repassivation. This type of metastable pitting usually appears in austenitic stainless steels [7] and in their welded joints, as is shown in this paper (Figs. 4 and 7). Stable pits in the welded joints are formed with a further increase in potential. The current density rapidly and continuously increases during the stable pit growth.
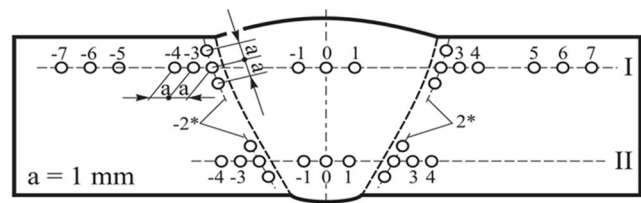
The values of the pitting corrosion indicators ($E_{pit} - E_{corr}$ and $E_{pit} - E_{prot}$) are determined from the recorded polarization curves and shown in Table 8. The values of E_{corr} before the pitting corrosion tests are relatively close. The nature of the E_{corr} on AISI 304 stainless steel in chloride and sulfate solutions was discussed previously [30].

The experimental values of the pitting corrosion indicators for the weld metal formed in the nitrogen-free and different amounts of nitrogen-containing shielding gas are shown in Table 7, for the welding current of 130 and 150 A. The results in Fig. 7 and in Table 7 show that welding current has a significantly lower influence on the indicators of pitting corrosion resistance ($E_{pit} - E_{corr}$ and $E_{pit} - E_{prot}$), than the nitrogen content in the shielding gas. Nitrogen from the shielding gas is dissociated in the arc column and dissolved in the (molten) weld pool. The nitrogen content dependence in the weld metal on the nitrogen content in the shielding gas is shown in Fig. 8 for the welding current of 130 A. Values of the welding parameters (Table 1) were constant during welding, so it was possible to expect linear dependence between the nitrogen content in the shielding gas and the nitrogen content in the weld metal (for the selected range of nitrogen content in the shielding gas). The obtained dependence between the nitrogen content in the shielding gas and the nitrogen content in the weld metal is shown in Fig. 8. However, it was not possible to precisely define the type of this dependence, because there were not enough experimental data.

Figure 9 shows the dependence of the pitting corrosion resistance on the nitrogen content in the weld

Table 5 Average value of ferrite numbers

I (A)	Ferrite number (FN_{av})		
	Ar	Ar + 1.25 vol% N_2	Ar + 2.50 vol% N_2
130	9.3	3.0	1.8
150	9.8	3.2	2.1

Fig. 3 Positions of hardness measurements (scheme)

Table 6 Results of hardness measurements

Shielding gas	I (A)		HV 10										
			Base metal	HAZ			Weld metal			HAZ			Base metal
			−7	−4	−3	−2*	−1	0	1	2*	3	4	7
Ar	130	I	201	201	183	178	181	181	181	177	177	186	191
		II	–	172	181	178	181	181	172	195	201	196	–
Ar + 1.25 vol% N_2		I	212	193	166	171	177	177	168	171	177	201	206
		II	–	212	201	183	186	186	186	184	191	181	–
Ar + 2.50 vol% N_2		I	203	200	186	175	186	191	188	169	166	198	201
		II	–	201	181	175	181	181	181	171	164	164	–
Ar	150	I	198	196	172	171	186	191	191	180	186	201	206
		II	–	188	186	177	164	172	172	177	181	196	–
Ar + 1.25 vol% N_2		I	206	196	198	181	181	181	181	177	181	203	206
		II	–	186	177	184	186	186	186	178	177	172	–
Ar + 2.50 vol% N_2		I	206	191	186	171	164	168	168	173	181	196	201
		II	–	181	168	167	191	186	191	175	172	181	–

metal. Figure 9a shows the dependence of the resistance to pit formation ($E_{pit} - E_{corr}$), and Fig. 9b shows the dependence of the resistance to pit growth ($E_{pit} - E_{prot}$) on the nitrogen content in the weld metal. Figure 9c shows the dependence of the pit formation indicator ($E_{pit} - E_{corr}$) on the pit growth indicator ($E_{pit} - E_{prot}$), for $I = 130$ A. Figure 10 shows the corresponding dependencies for the welding current $I = 150$ A.

Due to the relatively low PREN (pitting resistance number) and the presence of the ferrite and austenite phase (Figs. 5 and 6), the weld metal often shows a relatively high susceptibility to pit formation. Pits can be formed at the phase boundary austenite/ferrite in the weld metal [18]. With increasing of the nitrogen content


Fig. 4 Characteristic polarization curve with indicators of pitting corrosion

in the weld metal, the resistance to pit formation increases, but the resistance to pit growth decreases. The greater difference ($E_{pit} - E_{prot}$) indicates less resistance to pit growth. There is still not an unambiguous answer whether it is more important for the safety of the construction that austenitic stainless steels have less resistance to pit formation or less resistance to pit growth. Obviously, this depends on the chemical composition and corrosive media interdependency as well as on the surface roughness. According to ISO 15158 [23], the resistance to pitting corrosion of the austenitic stainless steels is determined based on the resistance to pit formation (E_{pit}). The resistance of austenitic stainless steels to crevice corrosion is determined according to the ASTM G78 standard [31]. The resistance to crevice corrosion has been shown to be in direct correlation with the resistance to pit growth [14], because both initiation mechanisms are quite similar. According to the ASTM F2129 standard [12], the resistance of austenitic stainless steels to pitting corrosion is determined on the basis of both indicators (E_{pit} and E_{prot}).

As it can be seen in Figs. 9 and 10, the values of $E_{pit} - E_{corr}$ are higher for the weld metal which contains more nitrogen than for the weld metal with less nitrogen. The decrease in the acidity of the solution within the pit, i.e., the increase of pH value due to the formation of ammonia ions in the presence of nitrogen, explains a higher resistance to pit formation in the weld metal [19–21]. In addition, the fraction of δ-ferrite in the weld metal is reduced in the presence of nitrogen. This has a favorable effect on the weld metal resistance to pitting corrosion. It can be seen in Figs.
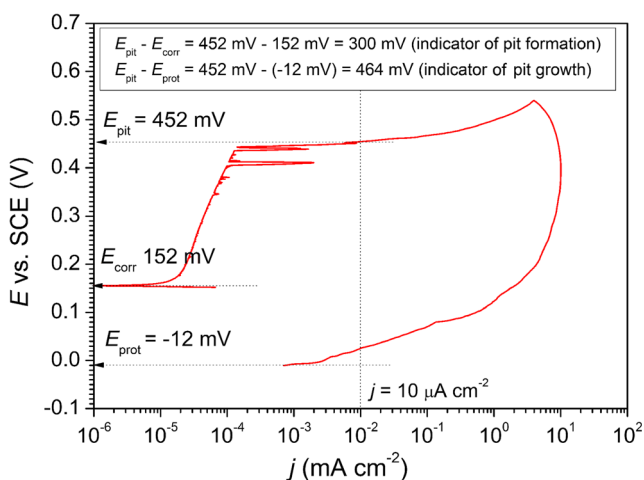
Fig. 5 Microstructure of weld metal formed in the shielding gas **a** without N₂, **b** with 1.25 vol% N₂, and **c** with 2.50 vol% N₂ (I = 130 A) (Adler's etchant)
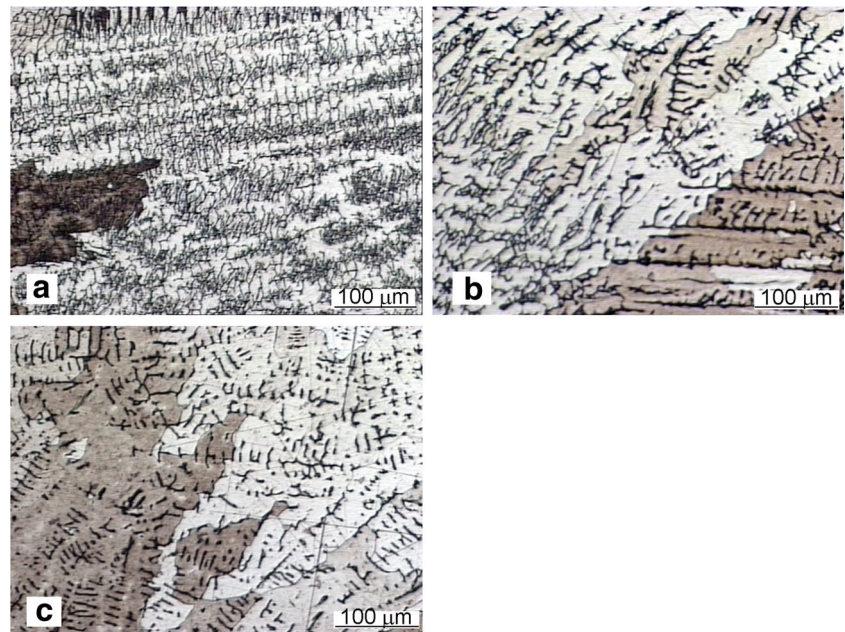

5, 6, and 11 that the content of δ-ferrite in the weld metal strongly depends on the nitrogen content in the shielding gas. Nitrogen as a strong austenite former is often used as an alloying element in duplex stainless steels in order to regulate their microstructure and to increase their resistance to pitting corrosion [18]. Austenitic stainless steels alloyed with nitrogen are also commercially produced.

After welding in the nitrogen-free shielding gas, the content of δ-ferrite (i.e., FN) in the weld metal was 9.3. During welding in the shielding gas with 1.25 vol% nitrogen, the FN decreases to 3.0, while in the case of the shielding gas with 2.50 vol% nitrogen, the FN decreases to 1.8 (Table 5). The chromium content in δ-ferrite is higher than the average chromium content in the weld metal. The presence of nitrogen in the weld metal resulted in a decrease in the fraction of δ-ferrite (rich in chromium). This led to a higher amount of austenite in the weld metal, and the chromium content was more homogeneous. δ-Ferrite is a chromium sink that reduces the amount of dissolved chromium atoms in the austenite matrix, which results

Fig. 6 Microstructure of weld metal formed in the shielding gas **a** without N₂, **b** with 1.25 vol% N₂, and **c** with 2.50 vol% N₂ (I = 150 A) (Adler's etchant)
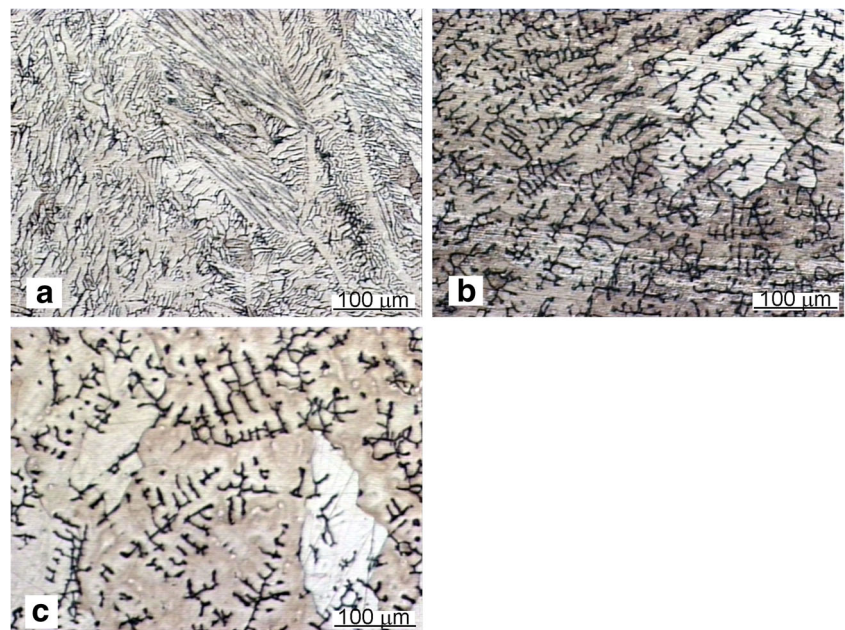
Fig. 7 Potentiodynamic polarization curves on the weld metal formed in the shielding gas **a** without N_2, **b** with 1.25 vol% N_2, and **c** with 2.50 vol% N_2 ($I = 130$ A and $I = 150$ A)
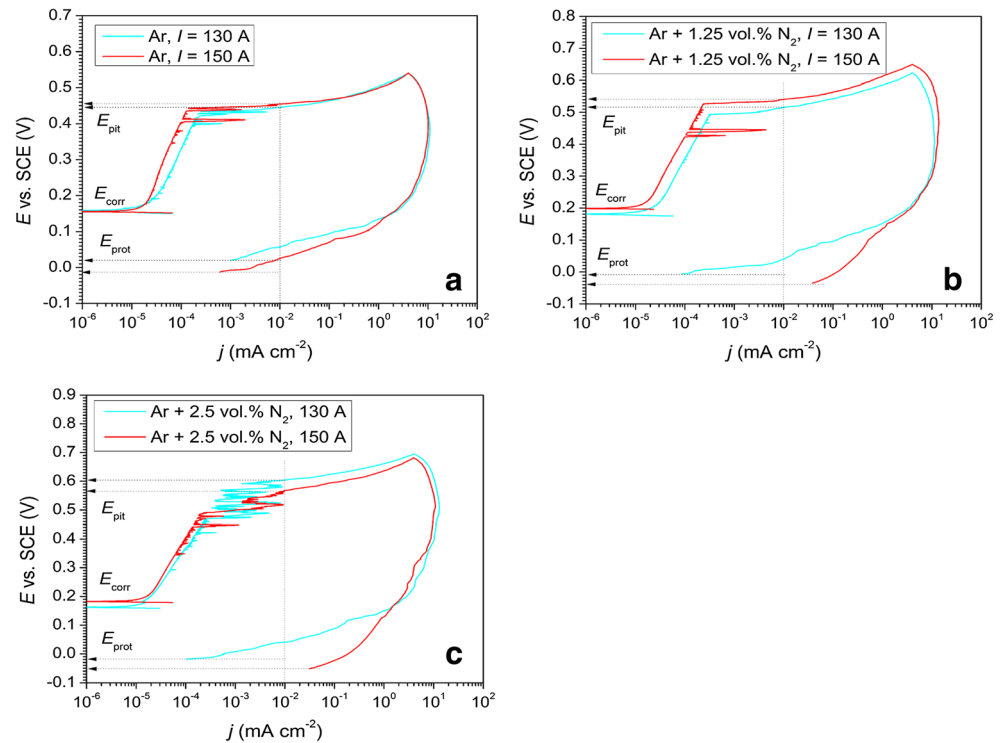
3.3 SEM/EDS

The concentration of chromium and other alloying elements in the weld metal was determined by SEM/EDS measurements. The dark and bright fields in Fig. 11 represent the ferrite phase and the austenite phase, respectively. Table 8 shows the typical results of the performed SEM/EDS measurements.

Table 8 shows that the concentration ratio Cr/Fe in the austenite phase increases when the nitrogen content in the shielding gas increases (spectrum 2). The

concentration ratio Cr/Fe in the ferrite phase has an approximately constant value, regardless of the nitrogen content in the weld metal (spectrum 1). An increase in the Cr/Fe concentration ratio in the austenite phase is a result of a less fraction of the ferrite phase (rich in chromium) in the weld metal, when the nitrogen content increases.

Pit formation in the weld metal is easier at the ferrite/austenite phase boundary. In the presence of nitrogen, the microstructure of the weld metal becomes more homogenized, the distribution of alloying elements becomes more uniform, and the surface of the ferrite/austenite phase boundaries is reduced (Figs. 4, 5, and 11). The difference between the ferrite and austenite phase composition is less and also the difference between the electrode potentials of these

Table 7 Indicators of pitting corrosion

	I (A)	E_{corr} (mV)	E_{pit} (mV)	E_{prot} (mV)	$E_{pit} - E_{corr}$ (mV)	$E_{pit} - E_{prot}$ (mV)	N_{WM} (mass %)
Ar	130	158	442	18	284	424	0.056
Ar + 1.25 vol% N_2		181	516	− 6	335	522	0.130
Ar + 2.50 vol% N_2		162	604	− 22	442	628	0.190
Ar	150	155	455	− 14	300	469	0.083
Ar + 1.25 vol% N_2		198	538	− 39	340	577	0.132
Ar + 2.50 vol% N_2		182	568	− 56	386	624	0.171
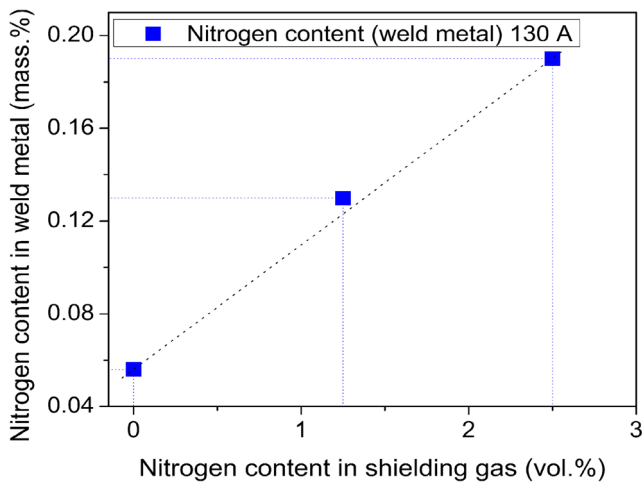
Fig. 8 Dependence of the nitrogen content in the weld metal on the nitrogen content in the shielding gas ($I = 130$ A)

phases. This results in a lower thermodynamic driving force for corrosion occurrence. All this leads to the increase of the resistance to pit formation in the weld metal. Also, as mentioned earlier, the acidity of the solution within the pit decreases in the presence of nitrogen due to the formation of ammonia ions, which also increases the resistance to pit formation.

It should be noticed that the presence of δ-ferrite in the weld metal is necessary for mechanical integrity of the welded joint. The content of δ-ferrite should be

3 to 15% [18]. The susceptibility of welded joints to hot cracking is significantly less in the presence of δ-ferrite in the weld metal.

In the presence of nitrogen, the resistance to pit formation in the weld metal is significant although the weld metal does not contain molybdenum, so that the synergetic effect of nitrogen and molybdenum is missing. A filler metal with a higher content of Cr and Ni, compared to their content in the base metal, was applied in this work, because of burn-off losses during welding (Table 2). Thus, a similar pitting corrosion resistance of the weld metal (without nitrogen) was obtained as that of the base metal. Results of pitting corrosion testing of the austenitic stainless steel X5CrNi18-10 (base metal) are presented in our previous paper [33]. The use of a filler metal with Mo was not necessary in this work. In the case of Mo-grade austenitic stainless steels, slightly alloyed Mo-grade filler metal must be applied (also due to burn-off losses during welding).

As mentioned before, with an increase in the nitrogen content in the weld metal, its resistance to pit formation increases ($E_{pit} - E_{corr}$ value increases), while the resistance to pit growth decreases. The resistance of the weld metal to pit growth is less because the difference $E_{pit} - E_{prot}$ is higher. The results presented in this paper are also the confirmation of the new theory of pitting corrosion proposed by Frankel, Li, and

Fig. 9 Dependence of **a** $E_{pit} - E_{corr}$ and **b** $E_{pit} - E_{prot}$ on the nitrogen content in the weld metal, and the dependence of **c** $E_{pit} - E_{corr}$ on $E_{pit} - E_{prot}$ ($I = 130$ A)
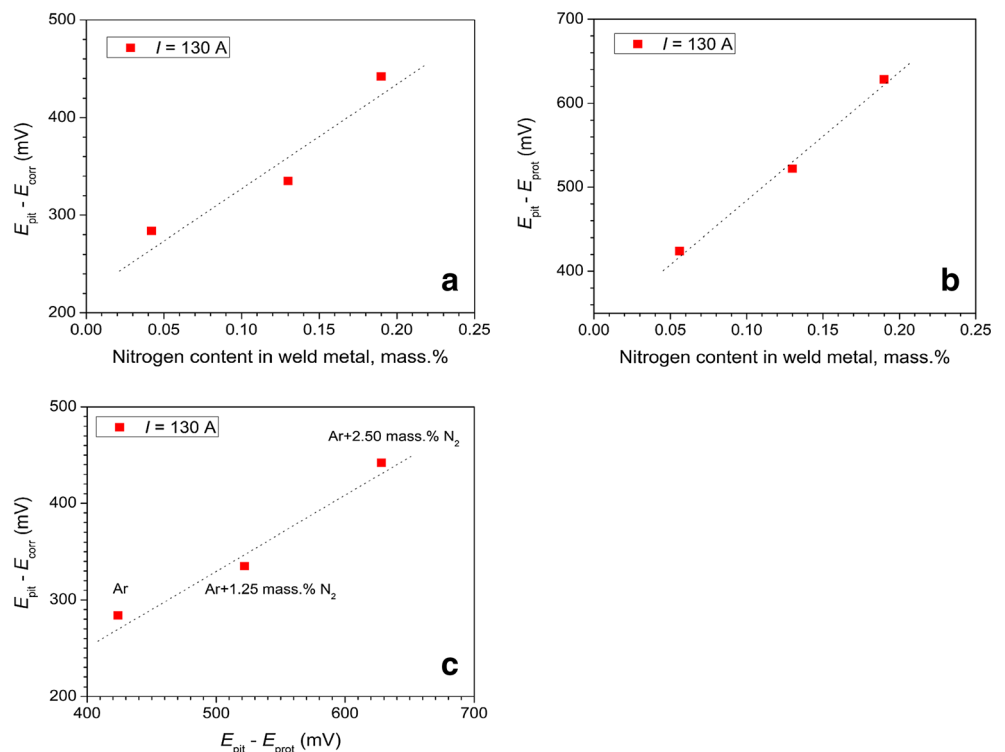
Fig. 10 Dependence of **a** $E_{pit} - E_{corr}$ and **b** $E_{pit} - E_{prot}$ on the nitrogen content in the weld metal and the dependence of **c** $E_{pit} - E_{corr}$ on $E_{pit} - E_{prot}$ ($I = 150$ A)
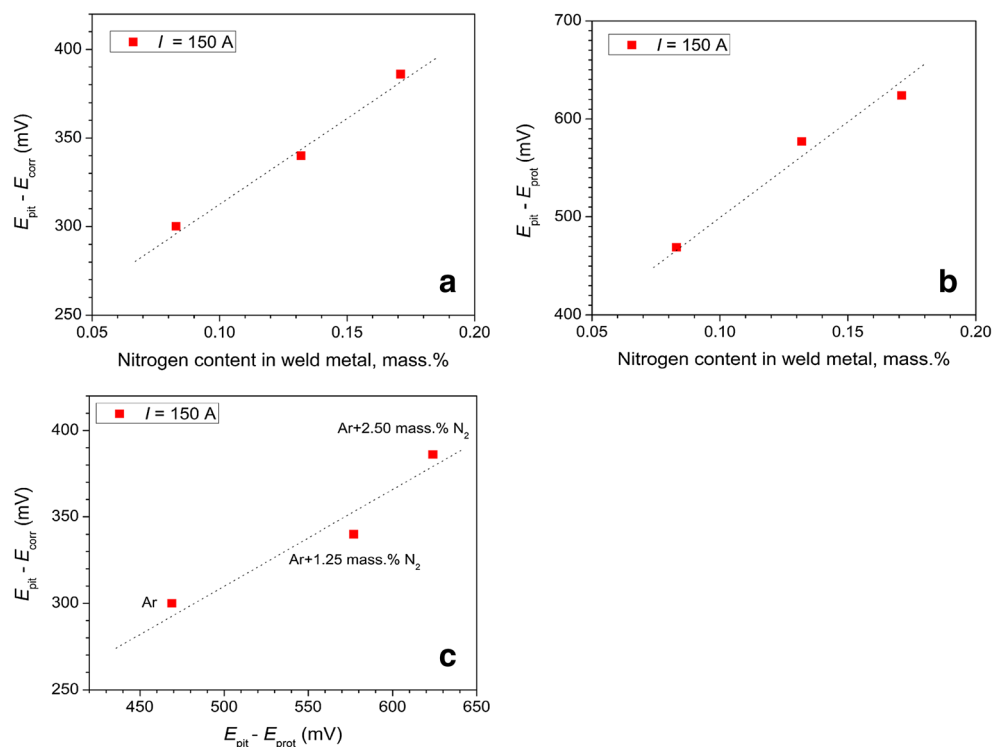
Scully [17]. In accordance with the proposed theory, if the resistance of a stainless steel to pit formation is greater, the resistance of this stainless steel to pit growth is less. In this case, the formed pits grow faster, i.e., their repassivation is more difficult. The presence of nitrogen increases the resistance of the weld metal to pit formation and reduces its resistance to pit growth.

Although the results presented in this paper are consistent with the proposed theory of pitting corrosion [17], the physical essence of the processes that lead to increased susceptibility of the weld metal to pit growth compared to the weld metal without nitrogen is still insufficiently clear. It can be assumed that a large difference between a pitting potential value and a corrosion potential value ($E_{pit} - E_{corr}$) is a thermodynamic driving force that facilitates pit growth. The thermodynamic driving force (ΔG) for corrosion occurrence is directly proportional to the potential difference ΔE ($\Delta G \sim \Delta E$). A good example is galvanic corrosion where a thermodynamic driving force strongly depends on the potential difference between metals in a galvanic contact.

4 Conclusion

The influence of welding parameters on pit initiation and pit growth in welded joints of X5CrNi18-10

stainless steel was studied. The obtained results showed that welding current and arc energy have a significantly lower influence on the resistance to pit formation and pit growth, than the nitrogen content in the shielding gas. Welding current and arc energy input are typical working parameter windows for welding of stainless steels.

The key factor for pit initiation and pit growth is the content of nitrogen in the shielding gas. The potentiodynamic polarization method was used for testing of the pitting corrosion resistance. It was shown that the resistance to pit formation in the weld metal was higher when welding was performed in a nitrogen-containing shielding gas. With an increase of the nitrogen content in the shielding gas, the nitrogen content in the weld metal increases almost linearly. In the presence of nitrogen, the fraction of δ-ferrite is reduced, as well as the ferrite/austenite phase boundary area. The chromium distribution becomes more uniform due to the homogeneous microstructure. Consequently, the resistance of the weld metal to pit formation is increased.

Due to the formation of ammonia ions in the presence of nitrogen in the weld metal, the acidity of the solution within the pit decreases, which also increases the resistance to pit formation. With the increase of the nitrogen content in the shielding gas, the resistance of the weld metal to pit growth decreases. It can be assumed that a large difference between the values of
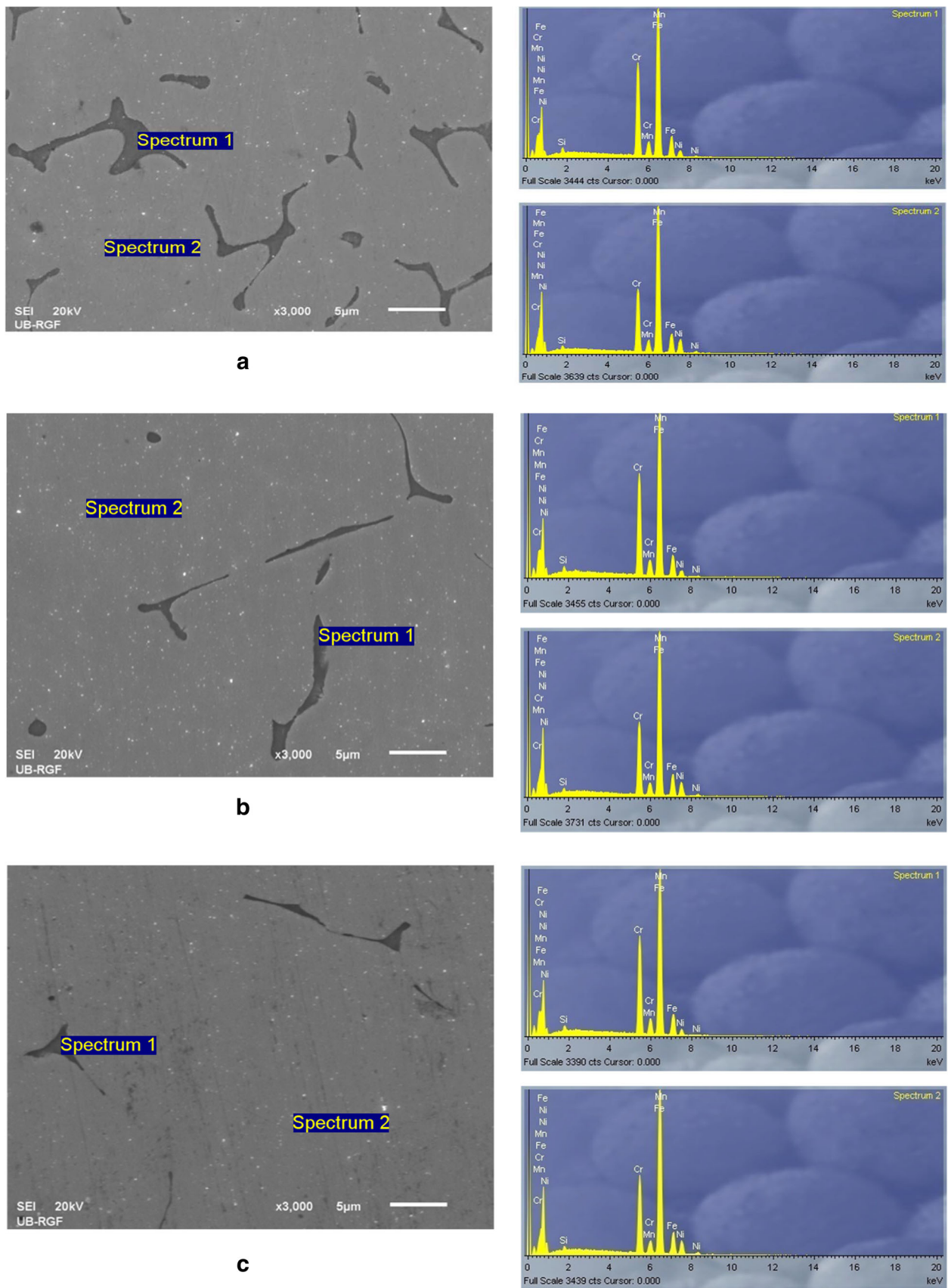
Fig. 11 SEM/EDS for the weld metal formed in the shielding gas: **a** without N$_2$, **b** with 1.25 vol% N$_2$, and **c** with 2.50 vol% N$_2$ (I = 130 A)

Table 8 Cr and Fe content in the ferrite and austenite phase, for the weld metal ($I = 130$ A)

		Cr	Fe	Cr/Fe (%)
Ar	Spectrum 1	25.5	68.7	37.1
	Spectrum 2	18.8	69.8	26.9
Ar + 1.25 vol% N_2	Spectrum 1	25.5	67.7	37.7
	Spectrum 2	19.1	69.4	27.5
Ar + 2.50 vol% N_2	Spectrum 1	25.5	68.9	37.0
	Spectrum 2	19.5	69.3	28.1

pitting potential and corrosion potential is a thermodynamic driving force that makes pit growth easier. Summarized, the presence of nitrogen increases the resistance of the weld metal to pit formation and reduces its resistance to pit growth. This is consistent with the proposed new theory of pitting corrosion.

References

1. Grubb JF (2005) Corrosion of wrought stainless steels. In: Cramer SD and Covino BS (eds.) ASM handbook, volume 13B: corrosion: materials, ASM International, Materials Park, pp. 54–77, doi: https://doi.org/10.1361/asmhba0003812

2. Aoki S, Sakamoto T, Zaizen T, Ogawa T (1982) The weldability of nitrogen-containing austenitic stainless steel: part I—chloride pitting corrosion resistance. Weld J 61:139–148

3. Jegdić B, Bobić B, Nedeljković D, Alić B (2017) Influence of welding current intensity on pitting corrosion resistance in welded joint of stainless steel X5CrNi18-10. Zasch Mater 58:297–303. https://doi.org/10.5937/ZasMat1703297J

4. Galvele JR (1976) Transport processes and the mechanism of pitting of metals. J Electrochem Soc 123:464–474

5. Suzuki T, Yamabe M, Kitamura Y (1973) Composition of anolyte pit anode of austenitic stainless steels in chloride solution. Corrosion 29:18–22. https://doi.org/10.5006/0010-9312-29.1.18

6. Frankel GS (1998) Pitting corrosion of metals. A review of the critical factors. J Electrochem Soc 145:2186–2198. https://doi.org/10.1149/1.1838615

7. Soltis J (2015) Passivity breakdown, pit initiation and propagation of pits in metallic materials—review. Corros Sci 90:5–22. https://doi.org/10.1016/j.corsci.2014.10.006

8. Pettersson CO, Boellinghaus T, Kannengiesser T (2007) Corrosion testing of welds, a review of methods. Weld World 51:79–106 Doc. IIW-1804-07 (ex-doc. IX-2197-06/IX-H-635-06)

9. Holmberg B, Bergquist A (2008) Suitable corrosion test methods for stainless steel welds. Weld World 52:17–21 Doc. IIW-1880-07 (ex-doc. IX-2230r1-07/IX-H-660-07)

10. Standard test method for conducting cyclic potentiodynamic polarization measurements for localized corrosion susceptibility of iron-, nickel-, or cobalt-based alloys—ASTM G61. doi:https://doi.org/10.1520/G0061-86R14

11. Tang Y, Zuo Y, Wang J, Zhao X, Niu B, Lin B (2014) The metastable pitting potential and its relation to the pitting potential for four materials in chloride solutions. Corros Sci 80:111–119. https://doi.org/10.1016/j.corsci.2013.11.015

12. Standard test method for conducting cyclic potentiodynamic polarization measurements to determine the corrosion susceptibility of small implant devices—ASTM F2129. doi:https://doi.org/10.1520/F2129-15

13. Corlett N, Eiselstein LE, Budiansky N (2010) Crevice corrosion, In Shreir's corrosion, fourth edition, Academic, Oxford, 753–771

14. Wilde BE, Williams E (1971) The relevance of accelerated electrochemical pitting tests to the long-term pitting and crevice corrosion behavior of stainless steels in marine environments. J Electrochem Soc 118:1057–1062

15. Wilde BE, Williams E (1971) The use of current/voltage curves for the study of localized corrosion and passivity breakdown on stainless steels in chloride media. Electrochim Acta 16:1971–1985

16. Bethencourt M, Botana FJ, Calvino JJ, Marcos M, Rodriguez-Chacon MA (1998) Lantanoide compounds as environmentally friendly corrosion inhibitors of aluminium alloys: a review. Corros Sci 39:1803–1819 PII:S0010-938x(98)00077-8

17. Frankel GS, Li T, Scully JR (2017) Localized corrosion: passive film breakdown vs pit growth stability. J Electrochem Soc 164: C180–C181. https://doi.org/10.1149/2.1381704jes

18. Davis JR (2006) Corrosion of weldments. ASM International, Materials Park www.asminternational.org

19. Osozawa K, Okato N, Fukase Y, Yokota K (1975) Effects of alloying elements on the pitting corrosion of stainless steel, (B. Gijyutsu). Corros Eng 24:1–7

20. Osozawa K, Okato N (1976) Passivity and its breakdown on iron and iron based alloys, USA–Japan seminar, National Association of Corrosion Engineers, Houston

21. Jargelius-Pettersson RFA (1999) Electrochemical investigation of the influence of nitrogen alloying on pitting corrosion of austenitic stainless steels. Corros Sci 41:1639–1664 PII:S0010-938x(99)00013-x

22. Du Toit M, Pistorius PC (2003) Nitrogen control during the autogenous arc welding of stainless steel. Weld World 47:30–43 Doc. IIW-1618-03 (ex-doc. IX-H-565-03 / IX-2068-03)

23. Westin EM, Johansson MM, Pettersson RFA (2013) Effect of nitrogen-containing shielding and backing gas on the pitting corrosion resistance of welded lean duplex stainless steel LDX 2101 (EN 1.4162, UNS S32101). Weld World 57:467–476. https://doi.org/10.1007/s40194-013-0046-2

24. Sales AM, Westin EM, Jarvis BL (2017) Effect of nitrogen in shielding gas of keyhole GTAW on properties of duplex and superduplex welds. Weld World 61:1133–1140. https://doi.org/10.1007/s40194-017-0486-1

25. Welding-fusion-welded joints in steel, nickel, titanium and their alloys (beam welding excluded)—quality levels for imperfections—ISO 5817

26. Steel and iron—determination of nitrogen content—titrimetric method after distillation—ISO 10702

27. Welding consumables—wire electrodes, wires and rods for arc welding of stainless and heat-resisting steels—classification—EN 12072

28. Kotecki DJ (2013) Welding stainless steel—questions and answers: a guide for troubleshooting stainless steel welding-related problems, 1st edition. American Welding Society AWS, Miami, ISBN-13: 978-0-87171-298-9

29. Method of measuring the pitting potential for stainless steels by potentiodynamic control in sodium chloride solution—ISO 15158. www.iso.org

30. Jegdić B, Dražić DM, Popić JP (2008) Open circuit potentials of metallic chromium and 304 stainless steel in aqueous sulphuric acid solution and the influence of chloride ions on them. Corros Sci 50: 1235–1244. https://doi.org/10.1016/j.corsci.2008.01.012

31. Standard guide for crevice corrosion testing of iron-base and nickel-base stainless alloys in seawater and other chloride-containing aqueous environments—ASTM G78. doi:https://doi.org/10.1520/G0078-15

32. Lu BT, Chen ZK, Luo JL, Patchett BM, Xu ZH (2005) Pitting and stress corrosion cracking behavior in welded austenitic stainless steel. Electrochim Acta 50:1391–1403 www.elsevier.com/locate/electacta

33. Jegdić BV, Bobić BM, Radojković BM, Alić B (2018) Formation and growth of pits on X5CrNi18-10 austenitic stainless steel in presence of chlorides and sulphates. Mat Protection 59:92–99 http://idk.org.rs/wp-content/uploads/2018/03/11BORE-JEGDIC.pdf